GEO Satellite Image Navigation with Cloud Detection using Multispectral Payload Image Data ⋆

E. Zaunick * **K. Janschek** ** **J. Levenhagen** ***

* *Institute of Automation, Technische Universität Dresden, Dresden, Germany (Tel.: +49 351 463 31913, Fax: +49 351 463 37039, e-mail: edgar.zaunick@tu-dresden.de).*
** *Institute of Automation, Technische Universität Dresden, Dresden, Germany (e-mail: klaus.janschek@tu-dresden.de).*
*** *EADS Astrium GmbH, Friedrichshafen, Germany (email: jens.levenhagen@astrium.eads.net)*

Abstract: Earth observation from geostationary orbit requires extremely accurate pointing knowledge of the instrument. Due to misalignments, thermal distortion effects and uncertainties on the attitude and position, it is essential to use image information, to meet the stringent requirements. We developed a high accuracy attitude estimation system, which uses multispectral payload image data. The navigation system evaluates the shift of the image content and reconstructs the rotational motion of the satellite. The estimation results are filtered and fused with AOCS data. The geometrical image correction and registration of the satellite images is performed using the improved knowledge of the line of sight.
The reliability of image navigation depends fundamentally on the correct recognition of cloud areas in the image data. Clouds can cover the earth's surface and images can become incomparable as well as cloud motion can be interpreted as false satellite motion. Thus, a cloud detection algorithm has been developed, which is based solely on unregistered and non-calibrated image data. A multispectral analysis (MSA) algorithm has been implemented, which uses VIS and IR channels for cloud detection during day and night time. The paper presents a description of cloud detection algorithm, results of sensitivity analysis with respect to ground texture and lightning conditions and simulation results of the navigation performance under cloud conditions.

Keywords: Image Navigation, Image Motion Compensation, Optical Flow, Motion Estimation, Cloud Detection.

1. INTRODUCTION

Geostationary Earth observation weather satellites acquire multi-spectral images during operational mode using a line scanner. Satellite rotational and translational motion during the image acquisition phase cause geometrical image distortions. Currently this problem is solved by the principle of landmark tracking using ground control points (GCP). It uses feature recognition (e.g. edge detection) of shorelines Liu and Jezek (2004), Madani et al. (2004), river or roads Boge (2003) or terrestrial landmarks Lim et al. (2004) and it matches the detected features with corresponding reference features taken from a database, see Fig. 1. Significant contributors to the GCP based image navigation errors are landmark variations over time, image distortions (blur, lightning), imprecise knowledge of the landmarks absolute position and cloud coverage. Ground control points are locally distributed on the Earth surface and can provide only a limited number of information.

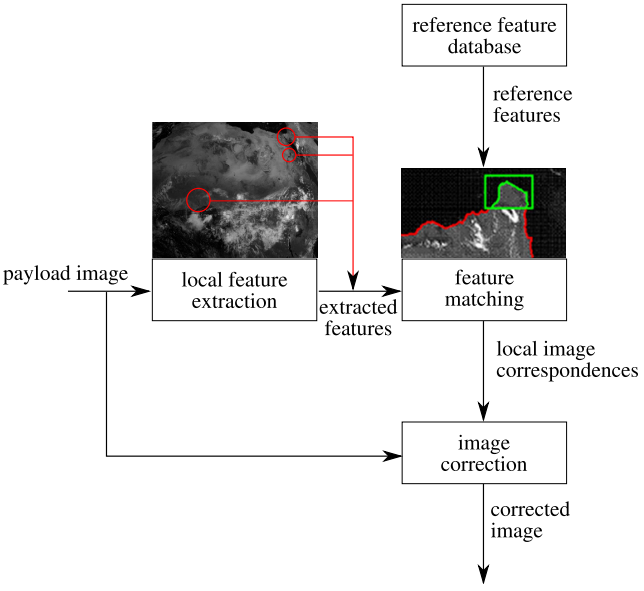

Fig. 1. GCP based Image Correction

⋆ Developed within a cooperation project between EADS Astrium GmbH Germany and Technische Universität Dresden.

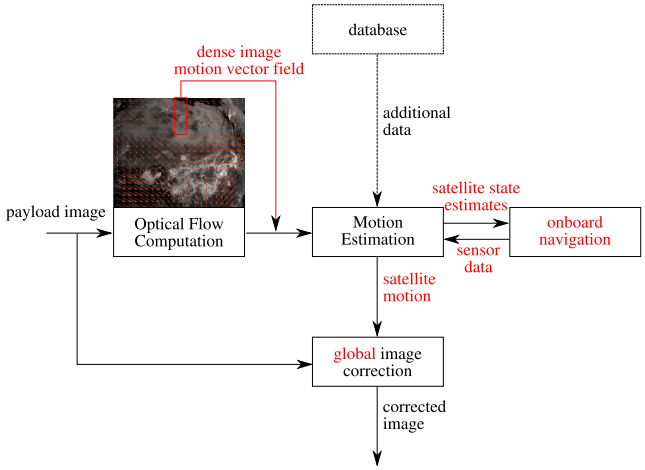

Fig. 2. Optical Flow based Image Correction

To overcome these limitations the current paper proposes an alternative attitude estimation approach using the whole image information of an imaging payload. The well known egomotion determination via optical flow (also image flow) processing Janschek et al. (2006), Tchernykh et al. (2006) is adapted to scan images Zaunick et al. (2008). This method offers several benefits against landmark tracking: it allows a robust and high accuracy determination of the satellite attitude as well as a geometrical correction of the payload scan images and it offers several variants with different level of a priori information, see Fig. 2.

Cloud coverage and cloud motion certainly disturbs the visual navigation estimation process. Clouds hide landmarks and they disturb the matching of image segments. Cloud motion can be interpreted as a false motion of image content and so mistaken as false satellite motion. In Saunders and Kriebel (1988) a series of threshold tests for AVHRR data (five spectral channels) have been developed. This algorithm has become a standard scheme for cloud detection. The use of both visible and IR channels allows a cloud detection during day and night time. Based on this standard scheme an improved cloud detection algorithm has been developed, which incorporates solely unregistered and non-calibrated image data and a multispectral analysis for discriminating cloudy and clear sky areas.

2. SYSTEM OVERVIEW

The system developed in our work, employs an attitude estimation system based on GEO satellite scanning imagery. The goal of the system is to estimate the 3D orientation of the camera coordinate frame, with respect to a global reference frame or relative to elapsed attitude histories. The system incorporates two types of navigational concepts: (a) the direct optical flow navigation (DOF), which uses two consecutively acquired images for navigation purposes without any complementary information and (b) the virtual optical flow navigation (VOF), which needs some a priori information. Both proposed image navigation methods use two images to compute the camera orientation. The first input image is the currently acquired camera image, whereas the origin of the second image differs for the two methods. In both cases the attitude determination is based on the image flow determination between the first and the second image. To compute the image flow a multipoint 2D correlation has been used.

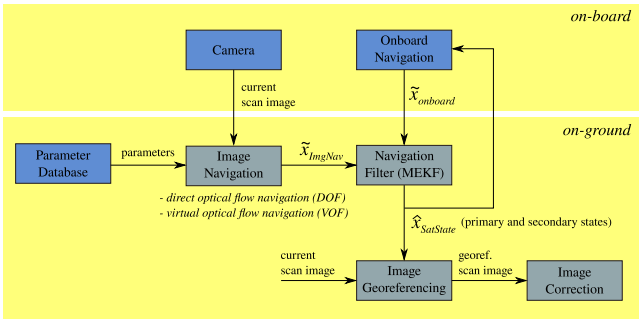

Fig. 3. System Architecture

Fig. 3 illustrates the system architecture. The images used in the image navigation (either DOF or VOF) are acquired by the payload (scanning imager) of the satellite. The current image and parameters (complexity depends on the method) are used to estimate the state vector of the camera. The state based on the image navigation is filtered and fused with the estimated state obtained from the on-board navigation (AOCS). Primary (e.g. attitude and angular velocity) and secondary states (e.g. rotations between coordinate systems and camera parameters) of the satellite are obtained after filtering. A side effect is the improvement of the overall state estimate of the satellite. Thus, the onboard navigation can be supported and the complexity of the AOCS can be reduced. Based on the improved satellite state the acquired image is georeferenced and geometrically corrected.

3. IMAGE NAVIGATION

The proposed image navigation methods are based on evaluating the movement of the image content (optical flow) by using a FFT block matching algorithm. For one pair of images [1] the optical flow is determined by subdividing both images into small fragments and 2D correlation of corresponding fragments. As a result of each correlation the local shift vector at the specific location is being determined, a whole set of local shift vectors forms an optical flow matrix. The reliability of each vector is determined by evaluating the height of the largest correlation peak, the relation of the highest to the second highest peak and by a boundary for the maximum shift magnitude. The image navigation method works with two different kinds of reference scans: (a) a previous scanned image or (b) a virtual image. Both concepts are described in the following subsections.

3.1 Direct Optical Flow Navigation

This variant does not need any a priori information and it employs the so called direct optical flow navigation between the current image and a previous scanned image. It gives a conclusion about the camera motion which took place between the acquisition instants.

The camera acquires a sequence of images during operational mode. Then the optical flow is computed between

[1] One pair of images consists of a reference image and a currently acquired image.

the current acquired image and a previously acquired one. Each image also serves as input for the cloud detection algorithm, which determines the visibility of the earth surface on the image. Thus, the computed optical flow field and the cloud mask form the inputs to the motion estimation algorithm. At those areas, where the earth is visible, the optical flow vectors are used to compute the rotation between the two images. There is no relation to a global frame and the two attitudes are independent from each other and from other frames. Therefore the computed rotation corresponds to a relative rotation between the two acquisition instants.

3.2 Virtual Optical Flow Navigation

This variant needs some a priori information: a preferably high accuracy geo-referenced image, an a priori camera pose estimate and surface data of the Earth (ellipsoidal parameters or digital elevation model). Fig. 4 shows the block diagram of the VOF navigation algorithm. In some way this method is similar to the DOF navigation, since one acquired image from the camera is used to compute the optical flow. But the second image is a synthetic image derived from an image generation block. Based on a reference image, the a priori camera pose estimate (taken from the last instance or the AOCS) and surface parameters of the earth, a so called virtual image is generated. This virtual image looks like if it was taken from the estimated camera pose. The principle of the image generation works like a ray tracing method. Considering the camera characteristics for each pixel a virtual line of sight (LOS) is computed. Based on the estimated pose of the camera and the geometrical shape of the earth the intersection points of each LOS with the earth can be determined. Thus, each pixel of the image plane gets a corresponding earth coordinate with respect to the ECEF. The grey value of each pixel is interpolated with data from the reference image. Observing the earth from geostationary orbit, the geometrical shape of the earth can be assumed as ellipsoidal.

The optical flow between the current acquired image and the generated image is computed using a 2D cross correlation algorithm. Cloud contaminated areas are detected using the cloud detection algorithm. Based on the image flow vectors of the visible areas the camera rotation is estimated. Since the computed rotation took place between the virtual and the current image, the result gives a conclusion about the difference between the estimated and the real camera orientation. Thus, the a priori camera orientation estimate is corrected based on the computed difference. The corrected camera pose can be used again to generate a new virtual image and the accuracy can be increased iteratively. In most cases, the algorithm converges after two or three iterations and the accuracy reaches a constant value. The yaw angle determination is very sensitive and also influences the other angles. Therefore the precision of the initial values directly drives the overall accuracy. Thus, importing the yaw angle from the AOCS and leaving it unchanged tends to make the algorithm more robust.

Although assuming the earth ellipsoidal, the computational effort to generate the virtual images is rather huge in

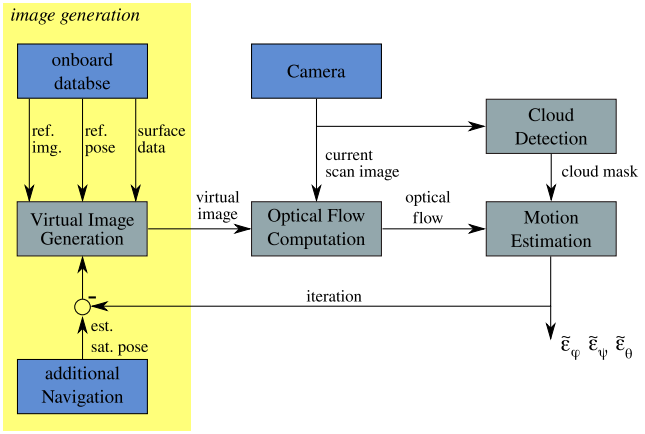

Fig. 4. Principle of Virtual Optical Flow Navigation (VOF)

comparison to DOF navigation where no image generation is required. Therefore the VOF method can not be used as real time application, unless preprocessed virtual images which are saved in a database or special image processing hardware, e.g. GPUs, is used for efficient computation.

4. ROTATION ESTIMATION

The computed optical flow gives a conclusion about the camera motion which took place between the acquisition instants of two images. Since the origin of the two images has no influence on the method how to compute the motion, the egomotion estimation described below is valid for DOF navigation as well as for VOF navigation. The rotation estimation is based on the well known egomotion equation

$$d\mathbf{x} = \frac{1}{z}\mathbf{A}(\mathbf{x}) \cdot d\mathbf{s} + \mathbf{B}(\mathbf{x}) \cdot d\Phi \qquad (1)$$

where $d\mathbf{x}$ denotes the image shift on the image plane, z is the z-component of the world point w.r.t. the camera frame, $d\mathbf{s}$ is the infinitesimal translational motion and $d\Phi$ denotes the infinitesimal rotational motion of the camera.

Since translational motion of the camera with respect to the ECEF (earth centered and earth fixed) frame is small and the distance to the scene points is very large, the effect of translational image flow can be neglected for the current application. Thus, (1) reduces to

$$d\mathbf{x} = \mathbf{B}(\mathbf{x}) \cdot d\Phi \qquad (2)$$

Equation (2) represents a linar system of equations, which characterises the projection of the camera rotation onto the image plane. If sufficient many image shift vectors $d\mathbf{x}$ are available, the camera rotation $d\Phi$ can be computed by solving (2). The computed rotation gives a conclusion of the satellite motion between the acquision phases of the two input images. For more detailles refer to Zaunick et al. (2008).

5. CLOUD DETECTION

Cloud cover and cloud motion could be misinterpreted as camera motion by the algorithm and should therefore be detected before motion estimation. The cloud detection algorithm must deal with unregistered imagery. The developed cloud detection algorithm is based on the assumption, that cloudy areas are colder and brighter than

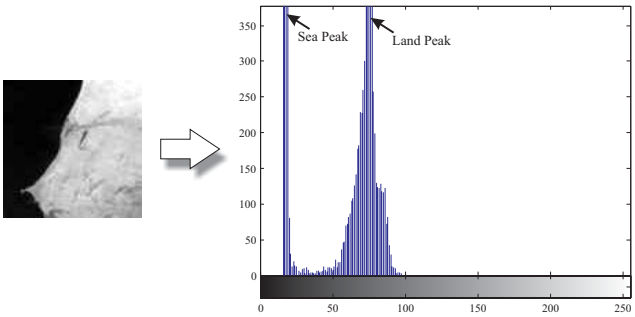

Fig. 5. Histogram of a cloud free coastal region (VIS8)

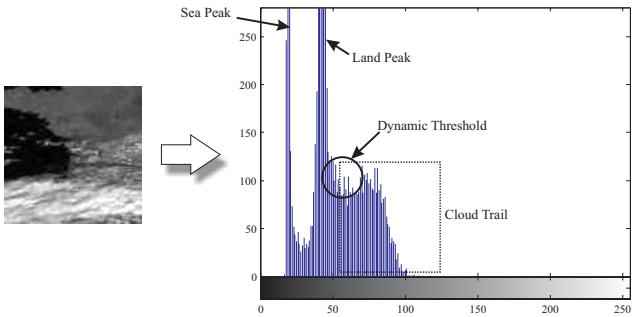

Fig. 6. Histogram of a cloud infected coastal region (VIS8)

clear-sky areas. Thus, the use of multiple channels allows to discriminate between clouds and clear sky areas during day and night time. For detailed reading refer to Klink (2008).

5.1 Multispectral Cloud Detection

Multispectral cloud detection is based on rather simple threshold tests, i.e. if the value of a pixel in one spectral channel is greater than a predefined threshold, then the pixel is regarded as cloud contaminated.

In general two subcategories of threshold tests exist: single channel tests and inter-channel comparison tests for which the channel differences are formed:

- IR10.8 . . . cold cloud test
- VIS8 . . . bright cloud test (during day only)
- VIS8 . . . bright cloud test (during day only)
- IR10.8 - IR12.0 . . . high cloud test
- IR8.7 - IR10.8 . . . cirrus cloud test
- IR3.9 - IR12.0 . . . thin cirrus test (during night only)
- IR10.8 - IR3.9 . . . low cloud and fog test

Furthermore it is very probable that the close-by pixels of a cloud infected pixel are cloudy as well. For these neighbouring pixels the same threshold test is exclusively run again but with a slightly lower/higher threshold.

5.2 Dynamic Threshold Determination

A major issue for these tests is to find appropriate threshold values. A common solution to this problem is to determine the thresholds dynamically from the scene content. Still, dynamic threshold determination remains difficult for coastal regions since there are usually large variations in albedo and surface temperature.

The developed algorithm is based on the assumption that cloud free images (both VIS and IR) have very characteristic spectral histograms. An image of a cloud free coastal region has two significant sharp peaks: a sea peak (dark, cold water) and a land peak (warmer, brighter). Fig. 5 and Fig. 6 show a cloud free and cloud infected landmark and their corresponding histograms. The algorithm will be further explained by means of a VIS8 image but it works in the same way for IR imagery. In case of IR imagery the histograms will look very similar while the order of peaks is inverted. Clouds are cold and therefore dark in contrary to their bright appearance in VIS imagery.

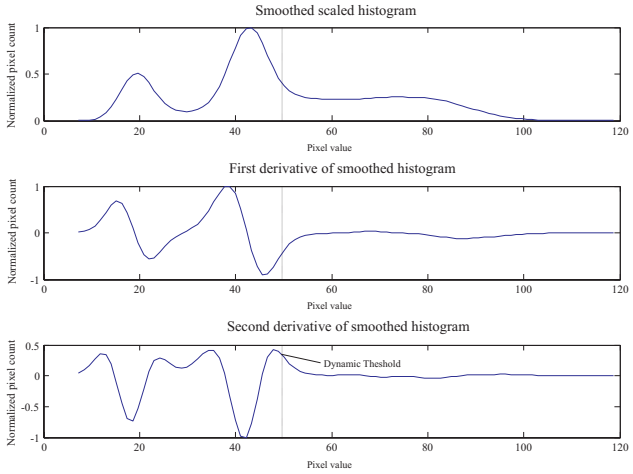

Fig. 7. Histogram Processing

An adequate threshold must have a higher value than the land peak and is therefore located at the foot of the land peak and at the beginning of the cloud trail. In a first step, the sea and land peaks need to be identified. The original histogram is smoothed to find unambiguous peaks. It is most likely that a histogram features three peaks: land, sea and clouds. Only scenes which are completely cloud free and have an utter homogeneous land surface or scenes in which one of the major elements (land or sea) is totally covered, feature two peaks. Scenes which are completely cloud covered show a single peak only.

The threshold is located at the base of the second peak which forms the land peak in the large majority of cases. The threshold is determined by finding the first maximum of the second derivative (greatest change in slope) of the smoothed histogram, see Fig 7. If the histogram features one distinctive peak only the threshold is found by multiplying the peak gray level with a static factor.

5.3 Generation of the Final Cloud Mask

Each test described in the previous sections creates a binary cloud mask. Since some tests tend to mark cloud free pixels as cloud contaminated or vice versa, a confidence factor for each test is introduced. The cloud mask of reliable tests such as the Cold Cloud test is weighted higher than the cloud mask created by the Spatial Coherence test. The weighted masks are merged into a single final cloud mask by calculating their sum. Finally a pixel is

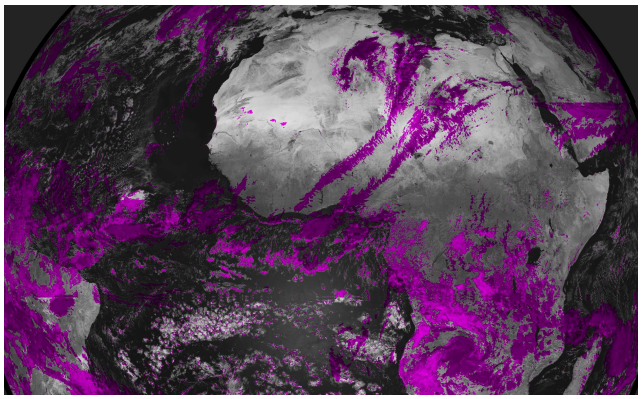

Fig. 8. Result of Cloud Detection during daytime

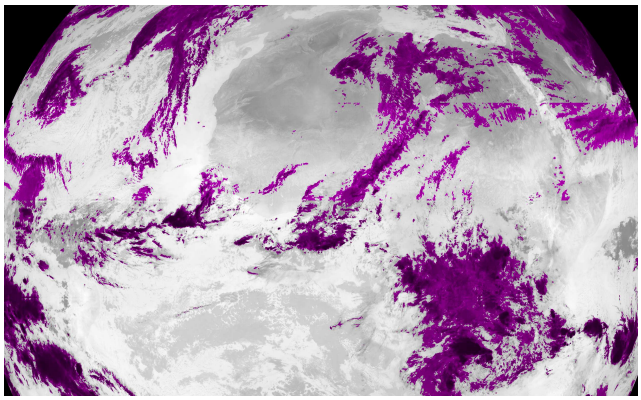

Fig. 9. Result of Cloud Detection during night

regarded as cloud contaminated if its value exceeds a static threshold.

6. SIMULATION RESULTS

6.1 Cloud Detection

The verification of the cloud detection scheme was performed manually since no reference cloud masks were available. The cloud conditions present in the landmark chips and the result of the cloud detection were inspected visually and categorized.

Fig. 8 and 9 illustrate two examples of the multispectral analysis during daytime and during night. The underlayed image shows the scanned area, the detected cloud mask is coloured in magenta. These tests have been accomplished with various image chips. Overall 222 chips have been inspected. The percentaged proportion of the weather conditions of the inspected images is depicted in Fig. 10 (left chart). The results of all verification tests (during day and night) are shown in Fig. 10 (right chart).

It can be summarized that the developed cloud detection scheme shows good results in more than 60% percent of the cases independent of the daytime or weather conditions. The algorithm tends to mark unnecessary pixels at daytime while only detecting a part of the clouds at night. This is probably due to the *Bright Cloud Test* which significantly contributes to the final cloud mask. The *Bright Cloud Test* is sensitive in scenes acquired at twilight or dawn. In general the cloud detection scheme

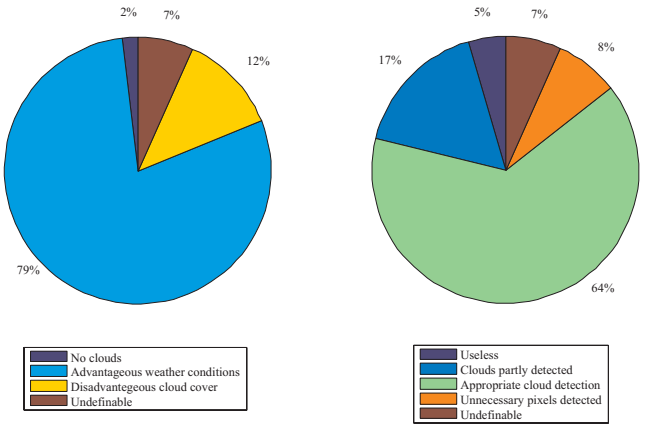

Fig. 10. Result of Cloud Detection during day and night

shows weaknesses in scenes which feature regions with a very high albedo, e.g. desert (very bright) and in scenes in which either land or sea is mostly covered by clouds. In the latter case clouds are misinterpreted as land area due to the dynamic threshold determination and therefore clouds will not be detected completely. It works best with scenes which feature a histogram with three peaks or two peaks with a distinctive cloud trail. However, even if too few or too many pixels have been marked as cloud contaminated, the remaining visible shoreline should serve as appropriate enough input data for the following edge detection and matching process. In just very few cases, 5%, the cloud detection algorithm returned completely false classification results.

6.2 Rotation Estimation

The effect of the *Cloud Detection* on the *Image Navigation* has been tested by applying the DOF Navigation. For this simulation real satellite imagery (MSG [2]) has been used. The repeat cycle of the acquisition phases between two images is $15min$. Thus, cloud motion and cloud coverage are real and not generated. An angular offset of $5 \cdot 10^{-3} rad$ is added to all axes to simulate the motion of the satellite.

Fig. 11 through Fig. 13 demonstrate the influence of cloud motion on the rotation estimation of each axis. The left charts show the image based attitude estimation without cloud detection. Cloud contaminated image chips do not move as they would move due to satellite motion. This leads to erroneous attitude estimation results. An unambiguous relationship exists between the optical flow field and the satellite motion after eliminating of cloud contaminated shift vectors (right charts Fig. 11 through Fig. 13). The accuracy of the estimated angles can be improved significantly. If no valid shift vector remains, the result is set to zero.

7. SUMMARY

The use of payload image information helps considerably improving the pointing knowledge of the instrument significantly. The more information is available the better is the performance of the determination of the line of sight. Therefore we developed a navigation system, which

[2] Meteosat 2nd Generation.

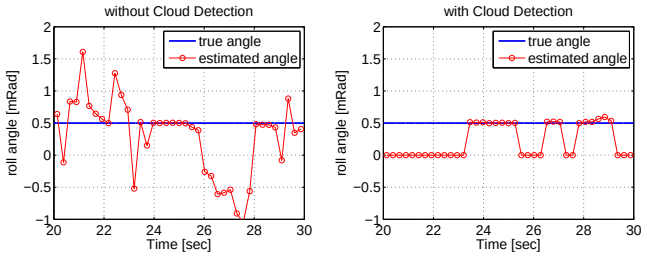

Fig. 11. Effect of Cloud Detection on Image Navigation results (roll angle), left: estimation without cloud detection, right: estimation with cloud detection

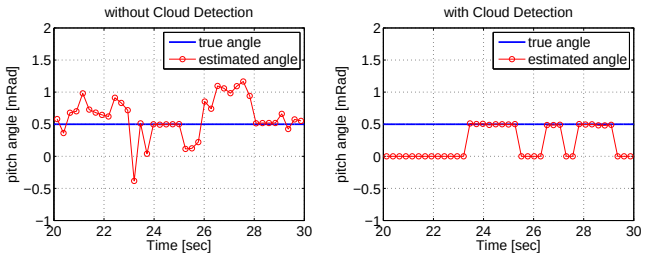

Fig. 12. Effect of Cloud Detection on Image Navigation results (pitch angle), left: estimation without cloud detection, right: estimation with cloud detection

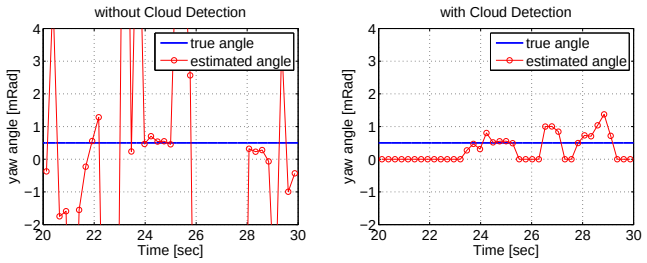

Fig. 13. Effect of Cloud Detection on Image Navigation results (yaw angle), left: estimation without cloud detection, right: estimation with cloud detection

uses the whole image information. The experiments have shown, that cloud coverage and cloud motion disturbs the precise reconstruction of the camera orientation. Reliable cloud detection during day and night time is essential to assure permanent high operation performance. The cloud detection scheme developed in our system is based on multispectral analysis of VIS and IR channels. Cloud contaminated image chips are eliminated. The accuracy and reliability of the system is increased significantly.

REFERENCES

Boge, T. (2003). *Bordautonome Navigation von LEO-Satelliten mittels Magnetometer- und Landmarkenmessungen*. Ph.D. thesis, Technische Universität Dresden, Fakultät Elektrotechnik und Informationstechnik.

Janschek, K., Tchernykh, V., and Beck, M. (2006). Performance analysis for visual planetary landing navigation using optical flow and dem matching. In *In Proceedings of the AIAA Guidance, Navigation and Control Conference*, AIAA-2006-6706. Keystone, CO.

Klink, V. (2008). *Implementierung eines Landmark-Tracking Verfahrens für geostationäre Beobachtungssatelliten*. Technische Universität Dresden.

Lim, Y.J., Kim, M.G., Kim, T., and Cho, S.I. (2004). Automatic precision correction of satellite images using the gcp chips of lower resolution. volume 2, 1394–1397 vol.2.

Liu, H. and Jezek, K.C. (2004). Automated extraction of coastline from satellite imagery by integrating canny edge detection and locally adaptive thresholding methods. *International Journal of Remote Sensing*, 25(5), 937–958.

Madani, H., Carr, J.L., and Schoeser, C. (2004). Image registration using autolandmark. *Geoscience and Remote Sensing Symposium, 2004. IGARSS '04. Proceedings. 2004 IEEE International*, 6, 3778–3781 vol.6. doi: 10.1109/IGARSS.2004.1369945.

Saunders, R.W. and Kriebel, K.T. (1988). An improved method for detecting clear sky and cloudy radiances from avhrr data. *International Journal of Remote Sensing*, 123 – 150.

Tchernykh, V., Beck, M., and Janschek, K. (2006). Optical flow navigation for an outdoor uav using a wide angle mono camera and dem matching. In *In Proceedings of the 4th IFAC Symposium on Mechatronic Systems*, volume 4. MECHATRONICS, Heidelberg, Germany.

Zaunick, E., Janschek, K., and Levenhagen, J. (2008). Optical flow based geo satellite attitude estimation from payload image data. In *ESA Conference on Guidance, Navigation and Control Systems*. ESA, Trallee, Ireland.